J. Fluid Mech. (1987), *vol.* 177, *pp.* 407–436
Printed in Great Britain

Scanning currents in Stokes flow and the efficient feeding of small organisms

By S. CHILDRESS,
Courant Institute of Mathematical Sciences, New York University,
New York, NY 10012, USA

M. A. R. KOEHL
Department of Zoology, University of California, Berkeley, CA 94720, USA

AND M. MIKSIS
Department of Engineering Sciences and Applied Mathematics, Northwestern University,
Evanston, IL 60201, USA

(Received 29 November 1985 and in revised form 23 September 1986)

The feeding behaviour of many small, free-swimming organisms involves the creation of a scanning current by the coordinated movement of a group of appendages. In this paper, we study the generation of scanning currents in Stokes flow in a number of simple models, utilizing the movement of Stokeslets, spheres, or stalks to set up an average scanning drift in a suitable far-field formulation. Various mechanisms may then be classified by the rate of decay at infinity of the mean scanning current. In addition, optimal scanning can be investigated by minimizing the mean power required to create a current of prescribed amplitude. The simple mechanisms for scanning described here provide a framework within which the appendage movements of small aquatic organisms can be analysed and the relative merits of scanning and swimming strategies can be investigated.

1. Introduction

Many small, free-swimming organisms feed on particles of algae or detritus suspended in the water about them. These suspension feeders, which include protozoans, diverse invertebrate larvae, and planktonic crustaceans, encounter food particles by using movable appendages to locomote through the water or else to create local feeding currents allowing nearby water to be scanned. The appendages often operate at low Reynolds numbers (see e.g. Lochead 1977; Zaret 1980; Chia, Buckland-Nicks & Young 1981; Fenchel 1986), and it is therefore possible to use Stokesian hydrodynamics to estimate the power requirement for the feeding behaviour. If the feeding energy budget has been a factor in the evolution of these behaviours in various zooplankters, we might then expect the motions to be in some sense hydrodynamically efficient. This paper is concerned with several simple fluid-dynamical models of feeding with particular emphasis on behaviours that satisfy some criterion of optimality.

The principal focus of this paper is on the process of generating a 'scanning current'. We shall not address here the process of removing food particles that have come within the capture range of the organism (although at low Reynolds number this is also a problem of interest). In general terms, the problem we wish to consider

is the following: how should a small, free-swimming creature, endowed with a set of movable appendages, wave these about so as to 'scan' (i.e. cause to move past the organism or through some capture zone), with minimal expenditure of energy, a fixed volume of water per unit time? To study this question we shall explore a number of highly simplified models of appendage motion, in which this general question can be precisely formulated and, to some degree, answered.

Although all of our models are over-simplified when compared to the actual geometry of small organisms engaged in feeding behaviours, we suggest that a basic study of available Stokesian strategies is a necessary first step for understanding the variety of biological examples. The patterns of movement of feeding appendages can vary between species and between the life stages of one species. Moreover, various appendages on the body of a single organism can move in different ways, and one appendage can show several patterns of movement (e.g. Koehl 1984). It could well be that a hydrodynamically inefficient behaviour carries little penalty, but that premise can also be tested within the same class of models. Furthermore, it is important to remember that, for many small organisms, swimming is also a feeding behaviour, and it is of interest to understand when it might be preferred to move the body through the water, instead of the water past the body. For example, a clear case of scanning with no swimming occurs during hovering by an organism that would otherwise sink under gravity. (For neutrally buoyant bodies, we give an example in §6.) Indeed the class of problems that arise in the study of scanning are related to, but quite distinct from, certain questions of optimality arising in the theory of locomotion at low Reynolds number, and are perhaps closest to models of fluid transport by ciliated surfaces (Lighthill 1975). They are also closely related to studies of feeding by sessile, flagellated organisms (Higdon 1979*b*).

In §9 we consider some biological consequences of the physical scanning systems of small organisms predicted by our models. Our results can be used to investigate the relative merits of feeding strategies according to their hydrodynamic efficiencies.

2. Motion of a sphere in an infinite fluid

As noted in §1, scanning currents are frequently generated by periodic, almost clocklike motion of a group of feeding appendages. Possibly the simplest problem illustrative of the process replaces the appendage by a single sphere moving about in an infinite expanse of fluid. We assume that the time-independent Stokes equations govern the resulting motion of the fluid. Let the sphere have radius a. In order to realize a body of variable viscous resistance we allow a to depend upon time. While this will also introduce a volume change of little biological relevance, the model is representative of a large class of time-dependent Stokes flows in an exterior domain.

We suppose that the position vector of the centre of the sphere is $\boldsymbol{\xi}(t)$. Then the velocity $\boldsymbol{u}(\boldsymbol{x}, t)$ of the fluid at any point $\boldsymbol{x}$ exterior to the sphere is given by

$$\begin{aligned} u_i(\boldsymbol{x}, t) &= S_{ij}(\boldsymbol{x}-\boldsymbol{\xi})\,\dot{\xi}_j(t) + \dot{a}T_i(\boldsymbol{x}-\boldsymbol{\xi}) \\ &\equiv \tilde{u}_i(\boldsymbol{x}-\boldsymbol{\xi}(t), t), \end{aligned} \tag{1}$$

where, by the classical solution of Stokes (Batchelor 1967 p. 230)

$$S_{ij}(\boldsymbol{x}) = \tfrac{3}{4}a(t)\left(\frac{x_i x_j}{|\boldsymbol{x}|^3} + \frac{\delta_{ij}}{|\boldsymbol{x}|}\right) + \tfrac{1}{4}a^3(t)\left(\frac{\delta_{ij}}{|\boldsymbol{x}|^3} - \frac{3x_i x_j}{|\boldsymbol{x}|^5}\right), \tag{2a}$$

$$T_i(\boldsymbol{x}) = a^2(t)\left(\frac{x_i}{|\boldsymbol{x}|^3}\right). \tag{2b}$$

The first term on the right-hand side of (2*a*), involving two contributions which decay like $|\boldsymbol{x}|^{-1}$, comprise a Stokeslet effect of a concentrated force on the surrounding fluid, and is one of the infinite set of singular solution of Stokes equations derivable from symmetric and skew-symmetric fundamental solution tensors. For discussion of this general approach to exterior problems see Batchelor (1967, chapter 4), Blake (1971), Lighthill (1975, chapter 3), and Chwang & Wu (1975).

We now suppose that the sphere moves on a fixed closed orbit with fixed period T. (We must fix the period since it will turn out that a fixed scanning amplitude can be maintained at arbitrarily low power by sufficiently slow movement, this being a consequence of viscous dissipation being quadratic in the velocity, see below.) Since the force on the sphere is $\boldsymbol{F}(t) = 6\pi\mu a\dot{\boldsymbol{\xi}}$ while the radial viscous stress on the sphere, associated with the change of radius, is $-2\mu a^{-1}\dot{a}$, the work done over one orbit is

$$W = 2\pi\mu \int_0^T (3a\dot{\boldsymbol{\xi}}^2 + 4a\dot{a}^2)\,\mathrm{d}t, \tag{3}$$

where μ is the viscosity of the fluid. Our object is to minimize W over all closed orbits executed in period T, given that a certain measure of scanning amplitude is fixed.

According to (1), $\boldsymbol{u}(\boldsymbol{x}, t)$ has a complicated functional dependence upon $\boldsymbol{\xi}(t)$ and to simplify this as much as possible we consider the fluid in a neighbourhood of infinity, confining attention to a 'far field' where $|\boldsymbol{x}-\boldsymbol{\xi}| \gg L$, L being a length which characterizes the size of the orbit. To fix ideas and simplify the analysis we shall assume that $\boldsymbol{\xi}$ is periodic of period T and with zero mean, and that the orbit size is much larger than the size of the body being waved. That is, we let

$$\int_0^T \boldsymbol{\xi}(t)\,\mathrm{d}t = 0, \quad L = \max_{0 \leqslant t < T} |\boldsymbol{\xi}(t)| \gg \max_{0 \leqslant t < T} a. \tag{4}$$

Expanding $\tilde{u}_i$ in a Taylor's series we have

$$u_i(\boldsymbol{x}, t) = \tilde{u}_i(\boldsymbol{x}) - \frac{\partial \tilde{u}_i}{\partial x_k}(\boldsymbol{x})\,\xi_k + \frac{1}{2}\frac{\partial^2 \tilde{u}_i}{\partial x_k\,\partial x_l}(\boldsymbol{x})\,\xi_k\,\xi_l + \ldots. \tag{5}$$

The first term on the right-hand side of (5) contains the dominant fluid-dynamical effect of a moving sphere, given by the terms homogeneous of degree -1 in (2). This is again the Stokeslet term of (2). But it is evident that this term will average to zero over one period if a is constant. This simply says that motion of a rigid sphere on a closed orbit can produce no mean force on the fluid. By the same token, if $a(t)$ is allowed to vary, a net Stokeslet strength can arise over one period and the far field is dominated by this effective Stokeslet. This suggests that scanning behaviours can be characterized by the order of decay at infinity of velocity when averaged over an orbit. The dominant scanning current just described, involving a decay like $|\boldsymbol{x}|^{-1}$ will be called *first-order scanning*. One important example of first-order scanning is the flow field generated by a relatively heavy organism as it hovers in the fluid, since in this case the organism applies a force to the fluid equal to its weight. An example of second-order scanning, involving decay in the far field like $|\boldsymbol{x}|^{-2}$ is a free, neutrally buoyant organism. In that case the instantaneous force applied to the fluid is always zero, and sufficiently complicated movements can lead to non-zero terms which decay with the above estimate.

A formal definition of the order of a scanning behaviour should, however, take into consideration the fact that it is possible for the average particle drift in the far field to have no radial component. In such a case the particle will not move closer to the organism. We define the *scanning field* $\boldsymbol{U}(\boldsymbol{x})$ to be the average over a period of $\boldsymbol{u}(\boldsymbol{x}, t)$. Since this average is for fixed $\boldsymbol{x}$, Eulerian variables have been retained. Not only is

the Eulerian average the simplest to invoke here, it is also appropriate to the biological problem of feeding in a uniform suspension of food particles (or in a random environment with a uniform distribution of food particles). If a feeding strategy targeted a specific Lagrangian point representing an inertialess particle of food, then a Lagrangian average would be relevant and this would in general be distinct from the Eulerian one. Nevertheless, for the present model with assumption (4), the small amplitude of the Stokeslet velocity in the far field ensures that the Eulerian and Lagrangian averages agree to high order. We give details concerning this point in Appendix A.

The scanning field $\boldsymbol{U}$ is thus an auxiliary solenoidal flow field defined kinematically in the far field. In terms of $\boldsymbol{U}$, we now define nth-order scanning by the condition that $\boldsymbol{x}\cdot\boldsymbol{U}$ be $O(|\boldsymbol{x}|^{1-n})$ as $|\boldsymbol{x}|\to\infty$. The fact that only the radial component enters into this definition makes the scanning order different from the simple order of decay of the amplitude of the scanning field, a distinction which can be important in some circumstances (see §9).

The remainder of this section is devoted to an introductory example of third-order scanning, which results when a is constant, so the problem is one of moving a single rigid sphere on a closed orbit. Computing the derivatives in (5) using (2), and then averaging over one period, a mean Eulerian velocity field is obtained in the form

$$U_i(\boldsymbol{x}) \equiv \frac{1}{T}\int_0^T [S_{ij}\dot{\xi}_j + \tfrac{3}{2}a\dot{\xi}_i\,\boldsymbol{\xi}\cdot\boldsymbol{x}|\boldsymbol{x}|^{-3} - \tfrac{3}{4}a\dot{\xi}_i|\boldsymbol{\xi}|^2|\boldsymbol{x}|^{-3} + \tfrac{9}{4}a\dot{\xi}_i(\boldsymbol{\xi}\cdot\boldsymbol{x})^2|\boldsymbol{x}|^{-5}]\,\mathrm{d}t + O(aL^4T^{-1}|\boldsymbol{x}|^{-4}). \quad (6)$$

Since a is now constant the first term on the right-hand side of (6) contributes nothing, while the second and third terms yield terms of order $|\boldsymbol{x}|^{-2}$ and $|\boldsymbol{x}|^{-3}$ respectively. The second term, however, is seen to contribute no radial component to $\boldsymbol{U}$. We are thus left with

$$x_i\,U_i(\boldsymbol{x}) = -\tfrac{3}{4}a|\boldsymbol{x}|^{-3}\frac{1}{T}\int_0^T \dot{\boldsymbol{\xi}}\cdot\boldsymbol{x}\xi^2\,\mathrm{d}t + O(aL^4T^{-1}|\boldsymbol{x}|^{-3}). \quad (7)$$

This scanning mechanism is therefore third-order according to the above definition. Consequently a moving sphere has a weak effect in the far field. To introduce a measure of the amplitude of the scanning field, imagine a large spherical 'target zone' of radius $R \gg L$, within which particles are trapped and consumed. (We formally take R to be $O(|\boldsymbol{x}|)$, but regard it as actually a rather small zone in the far-field domain.) This would correspond, for example, to the zone around the body of a calanoid copepod within which it perceives a food particle and responds with a capture motion (Koehl 1984). The trapping rate is then proportional to the flux of food particles, as determined by the volume flux of the scanning field of fluid, $\dot{V}$ say, into the target zone. From (7) this flux crossing into the target sphere may be evaluated by integrating the radial component of the scanning field over that portion of the target sphere where it is negative, and we obtain $(3a\pi/4RT)\,|\boldsymbol{M}|$, where

$$\boldsymbol{M} = \int_0^T \xi^2\dot{\boldsymbol{\xi}}\,\mathrm{d}t \quad (8)$$

is a vector amplitude with dimensions L^3. The vector $\boldsymbol{M}$ is determined by the orientation of the movement of the body and, by (7), its orientation determines a hemisphere across which food particles will enter and may be trapped.

2.1. *Optimal motion in a plane*

From (8) it suffices to consider only those orbits which establish a vector scanning amplitude in a particular direction. Taking this direction to be parallel to the y-axis, we have $\boldsymbol{M} = (0, M, 0)$ as another constraint on the problem, in addition to the fixing of the period T. We therefore consider only orbits lying in the plane $z = 0, \boldsymbol{\xi} = (\xi_1, \xi_2, 0)$. To minimize W for fixed scanning amplitude, we seek extremals of $W - (6\pi\mu a\lambda)\, M \equiv \mathscr{F}$ where λ is a multiplier. Since now

$$M = \int_0^T \xi_1^2 \dot{\xi}_2 \, \mathrm{d}t, \tag{9}$$

the Euler equations are

$$\ddot{\xi}_1 + \lambda \xi_1 \dot{\xi}_2 = 0, \quad \ddot{\xi}_2 - \lambda \xi_1 \dot{\xi}_1 = 0. \tag{10a, b}$$

The solution of (10) in terms of elliptic functions is elementary, but since this problem is something of a prototype of our subject we give some details. Multiplying (10a) and (10b) by $\dot{\xi}_1$ and $\dot{\xi}_2$ respectively and adding we obtain

$$\dot{\xi}_1^2 + \dot{\xi}_2^2 \equiv q^2 = \text{constant}. \tag{11a}$$

A second integral follows from (10b):

$$\dot{\xi}_2 - \tfrac{1}{2}\lambda \xi_1^2 = -C = \text{constant}. \tag{11b}$$

Combining equations (11) and integrating to obtain $t(\xi_1)$, there results

$$\xi_1 = \left(\frac{2(q+C)}{\lambda}\right)^{\frac{1}{2}} \mathrm{cn}\left((\lambda q)^{\frac{1}{2}} t, \left(\frac{q+C}{2q}\right)^{\frac{1}{2}}\right), \tag{12}$$

in terms of the elliptic function $\mathrm{cn}\,(u, k)$.

To investigate how parameters are determined by T and M we first note that periodicity implies, from (11b), that

$$\int_0^T \xi_1^2 \, \mathrm{d}t = \frac{2CT}{\lambda}. \tag{13}$$

Thus the conditions that the period be T, and that (13) hold, yield two relations between the parameters. Since $C = (2k^2 - 1)\, q$, these take the form

$$T = (4/(\lambda q)^{\frac{1}{2}})\, K(k), \tag{14a}$$

$$T = (8/(\lambda q)^{\frac{1}{2}})\, (2k^2 - 1)^{-1} [E(k) - (1 - k^2)\, K(k)], \tag{14b}$$

in terms of the complete elliptic integrals E and K. From these two expresions we obtain a transcendental equation for k. From the tabulated values of the complete elliptic integrals we find that $k^2 = 0.83$ and $K(k) = 2.32$ approximately.

There remains the constraint imposed by fixing M. We have from (9) and (11b) that

$$M = \tfrac{1}{2}\lambda \int_0^T \xi_1^4 \, \mathrm{d}t - C \int_0^T \xi_1^2 \, \mathrm{d}t. \tag{15}$$

The second term on the right-hand side of (15) can be evaluated using (13). For the first term, we use (10a) and (11) as follows:

$$\int_0^T \dot{\xi}_1^2 \, \mathrm{d}t = \int_0^T \lambda \xi_1^2 \dot{\xi}_2 \, \mathrm{d}t = \int_0^T [q^2 - (\tfrac{1}{2}\lambda \xi_1^2 - C)^2] \, \mathrm{d}t = \lambda \int_0^T \xi_1^2 (\tfrac{1}{2}\lambda \xi_1^2 - C) \, \mathrm{d}t, \tag{16}$$

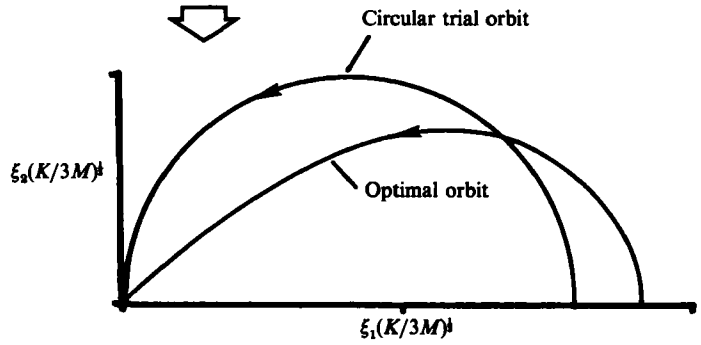

FIGURE 1. One-fourth of the optimal figure-of-eight motion of a sphere in a plane, compared with a figure-of-eight consisting of two circles. The latter is 12% less efficient than the optimal one according to the criterion (25), and 18% less efficient according to (35).

from which we obtain

$$\int_0^T \xi_1^4 \,\mathrm{d}t = \frac{4C^2T}{\lambda^2} + \tfrac{4}{3}q^2\frac{T}{\lambda^2}. \tag{17}$$

Thus (15) implies

$$M = \frac{2q^2T}{3\lambda} = \frac{(qT)^3}{24K^2}, \tag{18}$$

and we may use (14a) to express q in terms of M and T, giving

$$\left(\frac{K}{3M}\right)^{\frac{1}{3}}\xi_1 = k\,\mathrm{cn}\,(u,k), \quad u = \frac{4t}{TK}. \tag{19}$$

It can also be shown (see e.g. Jahnke & Emde 1945, chapters 5 and 6) that

$$\left(\frac{K}{3M}\right)^{\frac{1}{3}}\xi_2 = E(am(u),k) - \tfrac{1}{2}u. \tag{20}$$

These two expressions determine a figure-of-eight orbit shown in figure 1.

Let us now verify that the extremal defined by (19), (20) is indeed obtained at a local minimum of $\mathscr{F}$. The second variation is, with $(\delta\xi_1, \delta\xi_2) = (u, v)$,

$$\delta^2\mathscr{F} = \int_0^T [\dot{u}^2 + (\dot{v} - \lambda\xi_1 u)^2 - \tfrac{3}{2}\lambda^2\xi_1^2 u^2 + \lambda C u^2]\,\mathrm{d}t. \tag{21}$$

If we set $u = \dot{\xi}_1\phi(t)$ with ϕ periodic of period T, and use

$$\mathrm{d}(\ddot{\xi}_1)/\mathrm{d}t = \dot{\xi}_1(\lambda C - \tfrac{3}{2}\lambda^2\xi_1^2) \tag{22}$$

in (21) we obtain, after integrating by parts,

$$\delta^2\mathscr{F} \geqslant \int_0^T \dot{\xi}_1^2\dot{\phi}^2\,\mathrm{d}t \geqslant 0. \tag{23}$$

We are dealing here exclusively with functions of period T. The minimizing functions are thus seen to be

$$(u, v) = (\dot{\xi}_1, \dot{\xi}_2) \times \text{constant}, \tag{24}$$

and we see from (23) that $\delta^2\mathscr{F} = 0$. However (24) represents an infinitesimal shift of the sphere along its orbit, implying that $\delta^2\mathscr{F} > 0$ for any perturbation that is not simply a shift. In this sense a local minimum of $\mathscr{F}$ has been achieved.

Let us measure the efficiency of this scanning mechanism as follows: if $\dot{V}(R)$ is the

volume flow per unit time into a target sphere of radius R, as discussed above, we define the efficiency of scanning to be the dimensionless number

$$\eta = 4\mu W^{-1}\dot{V}(M^{\frac{1}{3}}). \tag{25}$$

For a far-field calculation, this value of η is based upon an extrapolation of the scanning field back to target zones comparable in size with the orbit. We must note, however, that the most reasonable definition of efficiency is not obvious and will depend upon the order of the scanning; we discuss this further in §3. In the present case, and with the definition (25), the optimal orbit yields, using (18),

$$2\eta = \frac{M^{\frac{4}{3}}}{(qT)^2} = (24K^2)^{-\frac{4}{3}} = 0.039. \tag{26}$$

For comparison consider the figure-of-eight orbit consisting of two touching circles of diameter L, the motion being again with constant speed q. For this orbit we have

$$T = \frac{2\pi L}{q}, \quad M = \pi L^{\frac{3}{2}}, \quad 2\eta = (4\pi)^{-\frac{4}{3}} = 0.034. \tag{27}$$

This is very close to the value for the optimal figure-of-eight. We superimpose this orbit on the optimal one in figure 1. We thus see that significant deviations from the optimal orbit do not change the efficiency very much.

We note in passing that (27) shows clearly how increasing the period for fixed scanning amplitude (here, fixed L) can lower the rate of working, the latter being proportional to q^2L, and thus shows why the period must be fixed to obtain a sensible optimization problem.

2.2. *Other results*

If the motion of the sphere is not constrained to lie in a plane, the optimal orbits are no longer figure-of-eight motions. Extending the above analysis, one obtains a family of spiralling orbits. If $\boldsymbol{M}$ is parallel to the z-axis, the optimal orbits are closed spirals $\boldsymbol{\xi} = (\rho\cos\theta, \rho\sin\theta, \xi_3)$ where

$$\dot{\xi}_3 = \tfrac{1}{2}\lambda\rho^2 - C, \quad \dot{\theta} = \frac{p}{\rho^2}, \quad \dot{\rho}^2 + \frac{p^2}{\rho^2} + \dot{\xi}_3^2 = q^2. \tag{28}$$

Note that the motion is again at constant speed. The additional integrations constant p determines the number of turns of the spiral over one period. These three-dimensional orbits are rather special and we shall not consider them further here. Nevertheless it is likely that most scanning behaviours, while not well represented by a single appendage, are essentially three-dimensional.

It is clear from (8) that $\boldsymbol{M}$ vanishes if the sphere is constrained to move on a spherical surface $|\boldsymbol{\xi}|^2 = L^2$. Since $\boldsymbol{M}$ is the amplitude of the field of radial motion, it can only vanish if on average the food particle remains a fixed distance from the organism. Such a behaviour would not aid an organism in feeding, and so this special case is of interest when one considers the waving about of some organelle connected to a fixed point by a rigid straight stalk. It is worth noting that the vanishing of $\boldsymbol{M}$ in this case is, in fact, independent of the far-field approximation, holding exactly for a Eulerian average velocity. To see this, one notes from (1) and (2) that, for fixed $\boldsymbol{x}, \boldsymbol{x}\cdot\boldsymbol{u}$ can be expressed as $\boldsymbol{x}\cdot\dot{\boldsymbol{\xi}}$ times a function of $|\boldsymbol{x}-\boldsymbol{\xi}|$ and $|\boldsymbol{\xi}|^2$. If the latter is constant, the time integral vanishes because of the differentiated factor. This result limits the usefulness of the single-sphere model, but the ideas introduced in this section can be readily extended to more realistic configurations.

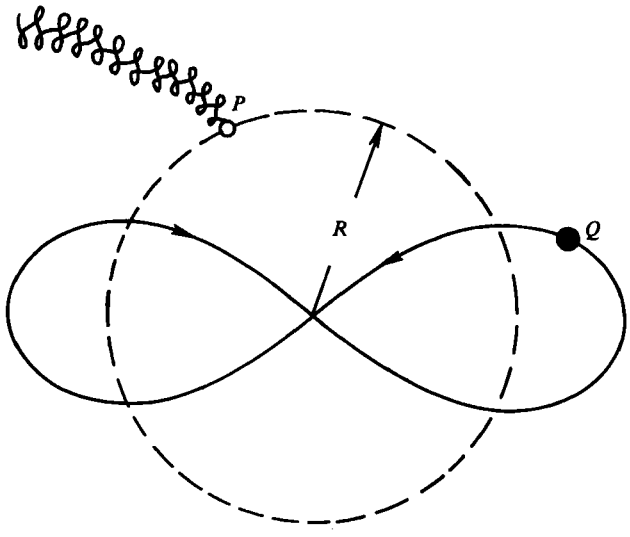

FIGURE 2. Third-order scanning by a sphere at Q leading to trapping of particle at P. The target zone is a sphere of radius R.

3. General considerations

The mechanism of induction of the scanning field in the single-sphere model can be understood by considering a single Lagrangian marker as shown in figure 2. The marker responds to the sphere by executing its own nearly closed figure-of-eight, but there are drifts due to variations in the velocity of the sphere and the separation distance PQ between the appendage and the particle. The first term on the right-hand side of (6) vanishes identically, and from the properties of the figure-of-eight orbit the scanning field has the form

$$\boldsymbol{U} \approx (\psi_{x_2}, -\psi_{x_1}, 0), \quad \psi = \left(\frac{3aM}{4T}\right) x_1 |\boldsymbol{x}|^{-3}. \tag{29}$$

This is a two-dimensional divergence-free flow in each plane $x_3 = \text{constant}$. This particular mechanism is the result of the symmetry of the sphere, the absence of any boundaries, and the fact that only one body is considered. None of these simplifications is really appropriate for the biological problem, and in subsequent sections we shall investigate how departures from the single-sphere geometry affect the scanning field.

As we have indicated in §2, it is useful to categorize scanning behaviour by the order of decay at infinity of the scanning velocity $\boldsymbol{U}(\boldsymbol{x})$. First-order scanning then occurs when there is a net Stokeslet strength in the scanning field. As we noted earlier, the most obvious natural example of scanning occurs in the 'hovering' of a negatively buoyant organism, for there the Stokeslet force is equal to the excess weight. A more artificial but simpler example is the waving about of an object whose resistance coefficient is variable (as the variable radius of the single sphere). It is perhaps preferable to replace the sphere by an arbitrary body whose orientation is adjusted along the orbit, in which case the leading term in (5) is changed to

$$u_i \approx S_{ij}(\boldsymbol{x})\, A_{jk}(t)\, \dot{\xi}_k. \tag{30}$$

where $\boldsymbol{A}(t)$ is a symmetric, positive definite matrix relating the velocity of the object to the point force $\boldsymbol{F}\delta(\boldsymbol{x}-\boldsymbol{\xi}(t))$ which replaces it in the far-field approximation. If we stipulate that a is now defined so that $\boldsymbol{A}$ has, say, determinant 1, we may write

$$F_i = 6\pi u a A_{ij}\dot{\xi}_j. \tag{31}$$

We shall discuss some two-dimensional examples of (30) in the following section.

For a free, neutrally buoyant organism, the scanning field that can be generated at some distance is necessarily of second or higher order, since the instantaneous net strength of the resultant Stokeslet must be zero. We consider some simple examples of this case in §6. For scanning of any order, there are significant new features when more than one appendage is utilized. We illustrate this for third-order scanning in §5. In §7 we discuss the related effect of the image system created when a boundary, such as the surface of the animal's body, is present.

We have noted above that the optimal movements of a single sphere of fixed radius have constant speed, and we show now that this is a general feature of optimal scanning. This will allow us to simplify the analysis of the more involved examples of first- and second-order scanning. Suppose that we have a neutrally buoyant organism having a complicated boundary (body, appendages, etc.), whose shape or orientation changes with time. We assume that a point on the boundary initially at $\boldsymbol{x}_0$ will subsequently have position $\boldsymbol{x}(f(t);\boldsymbol{x}_0)$ where

$$\boldsymbol{x}(0,\boldsymbol{x}_0) = \boldsymbol{x}(T,\boldsymbol{x}_0), \quad f(0) = 0, \quad f(T) = T, \quad f'(t) > 0.$$

A choice of $\boldsymbol{x}(f,\boldsymbol{x}_0)$ will fix the sequence of shapes parameterized by the artificial time f, while the choice of $f(t)$ determines the rate at which these shapes are realized in sequence over one period of the cycle. A helpful analogy is to imagine the sequence of shapes as images on a movie film strip. The running time of the film is fixed at T, but otherwise the speed of the projector is allowed to be varied at will.

Now it is well known (Happel & Brenner 1965) that, through the use of the Green function for the Stokes equations and the instantaneous boundary shape, the viscous dissipation within the fluid exterior to the body can be written as a quadratic functional of the boundary velocity:

$$W = \mathscr{W}[\dot{\boldsymbol{x}},\dot{\boldsymbol{x}}] = \int_0^T \dot{f}^2 Q(t)\,\mathrm{d}t = \int_0^T \phi(f)\,q(f)\,\mathrm{d}f, \quad \dot{f} \equiv \phi(f), \tag{32}$$

where $Q(t) = q(f(t)) > 0$ is determined by the boundary motion. Also, any measure of scanning amplitude, such as the amplitude of the far-field scanning velocity $\boldsymbol{U}(\boldsymbol{x})$, will be a linear functional of boundary velocity:

$$M = \mathscr{M}[\dot{\boldsymbol{x}}] = \int_0^T \dot{f}P(t)\,\mathrm{d}t = \int_0^T p(f)\,\mathrm{d}f. \tag{33}$$

Note that M is independent of f. We may then simply minimize W with respect to ϕ subject to the side condition

$$\int_0^T \frac{\mathrm{d}f}{\phi} = T. \tag{34}$$

It then follows that minimum dissipation occurs when $\phi = \text{constant} \times q^{-\frac{1}{2}}$ or $\dot{f}^2 Q = \text{constant}$. Thus the optimal motion corresponds to a constant rate of energy dissipation in the fluid, and correspondingly to a constant rate of working by the animal. As a general guide, therefore, whenever the energy cost of scanning is a

determining factor on the behaviour, and given that substantial changes in dissipation occur among competing movements, we should expect to see some variation in the speed of appendages accompanying changes in the resistance to motion which they experience. Movement should be slow when the resistance is large, fast when it is small, to maintain a constant rate of energy expenditure. We shall discuss some aspects of observed behaviours which bear on this question in later sections. Suffice it to say here that the simplest examples exhibit an insensitivity to the speed history and a rather broad minimum of W.

As we indicate in our discussion in §9, for many organisms of interest the assumption made here of Stokesian hydrodynamics is at best marginally valid; Reynolds numbers of appendage motion can in some species be near unity. For simplicity it seems reasonable in this case to base an approximate theory on Stokesian rather than inviscid hydrodynamics, with the understanding that inertial corrections should be added in some cases. We point out, however, that Oseen's classical criticism of Stokes' solution for a translating sphere does not apply to the scanning problem in the absence of mean motion of the organism, since the velocity at infinity is then zero relative to the body. If the instantaneous Stokes-flow velocity decays as $U(L/r)^{-N}$, the ratio of inertial to viscous force is $UL/\nu(L/r)^{N-1}$. Thus inertial corrections are needed throughout the flow only for a buoyant, hovering organism, and only then when local Reynolds numbers are not tolerably small. In all other cases $N > 1$ and so the effective Reynolds number decreases with distance. In particular, a far-field analysis is then consistent with the hydrodynamics, even though the far-field representation has been introduced mainly to obtain a relatively simple classification of scanning currents.

A final general point concerns the appropriate measure of scanning efficiency. The motivation behind (25) is reasonable but the choice $R = M^{\frac{1}{3}}$ is quite arbitrary. If instead we take

$$\eta = 4\mu W^{-1}\dot{V}(l) \quad (l = \text{orbit length}), \tag{35}$$

we obtain efficiencies of 0.0077 and 0.0063 for the optimal and circular orbits of figure 1. For second-order scanning, where the scanning field decays like $|\boldsymbol{x}|^{-2}$, $\dot{V}$ becomes independent of R and this ambiguity disappears. This is gratifying since for a neutrally buoyant, untethered organism the second-order mechanisms, involving zero net Stokeslet strength, are the strongest available. As we shall see in the next section, for first-order scanning the natural generalization of (25) which replaces R by $M^{\frac{1}{3}}$, is unreasonable, and when a single orbit is involved it is preferable to use (35). We suggest that (35) also be used for comparisons between scanning mechanisms of different order, when a single appendage is involved. For several appendages it is probably necessary to take into consideration the separation between orbits in the definition of R. We touch on this point in §5. All of these definitions necessarily involve only the far-field hydrodynamics, and it should be emphasized that this can only be very approximate when applied to specific organisms. Given that the actual target zone will be on the scale of the body geometry, a true efficiency cannot ignore near-field effects.

Although we shall frequently comment on orbit efficiency, we emphasize that, by definition, an efficiency is biologically significant only if significant gains to the organism are obtained by lowering the energy required to scan a given volume of water. This would presumably happen if scanning work comprised a significant fraction of metabolic activity, but it could also result from a fixed but small allocation to scanning, provided that the feeding rate was critical. Given the rewards of efficient scanning, we could expect evolution to optimize the behaviour, but a clear-cut

prediction of outcome based upon hydrodynamical principles is possible only if different scanning strategies have very different efficiencies. As we noted in §2, and just above for the optimality of constant rate of working, the simplest models exhibit a relative insensitivity in this regard.

4. First-order scanning by variable orientation

We now turn to the simplest examples of scanning with a non-zero mean Stokeslet component, producing first-order scanning according to the classification of the last section. To represent an appendage which changes its orientation as it moves on its orbit, we consider a matrix $\boldsymbol{A}$ in (30) with constant positive eigenvalues. If both the orbit and the function $\boldsymbol{A}(t)$ defined on it are fixed, we know from the previous section that the speed of the body for optimal scanning will make the dissipation rate a constant. The efficiency defined by (35) now has the form

$$\eta = \frac{Ml}{T\int_0^T \dot{\xi}_i \dot{\xi}_j A_{ij}\,\mathrm{d}t}, \tag{36}$$

where, given our freedom to choose the direction of the resultant $\boldsymbol{M}$, we have

$$\boldsymbol{M} = (M,0,0), \quad M_i = \int_0^T A_{ij}\dot{\xi}_j\,\mathrm{d}t. \tag{37}$$

To take the simplest case, suppose that motion is in the (x_1, x_2)-plane and the relevant 2×2 submatrix has eigenvalues λ_+, λ_- near unity, $\lambda_+ > \lambda_-$. Constancy of dissipation rate then implies that $|\dot{\boldsymbol{\xi}}| = \text{constant} = l/T$ to leading order in $|1-\lambda_+|$, and so (36) simplifies to an integral over arc length:

$$\eta = l^{-1}\int_0^l A_{ij}\tau_j\,\mathrm{d}s, \tag{38}$$

where $\boldsymbol{\tau}$ is the unit tangent vector. Let θ be the acute angle, measured counterclockwise, between the x_1-axis and the principal direction of $\boldsymbol{A}$ associated with λ_+. Then

$$\boldsymbol{A} = \begin{bmatrix} \alpha+\beta\cos 2\theta & \beta\sin 2\theta \\ \beta\sin^2\theta & \alpha-\beta\cos^2 2\theta \end{bmatrix} \quad (\alpha = \tfrac{1}{2}(\lambda_+ + \lambda_-), \quad \beta = \tfrac{1}{2}(\lambda_+ - \lambda_-)), \tag{39}$$

and so we obtain, with $\boldsymbol{\tau} = (\cos\psi, \sin\psi)$,

$$\eta = \frac{\beta}{l}\int_0^l \cos(2\theta-\psi)\,\mathrm{d}s. \tag{40}$$

Thus the optimal value of η is independent of path and is obtained by taking $\theta = \frac{1}{2}\psi$. We show some representative orbits in figure 3, taking the object to be a flat plate. Note that for continuous motions the circular orbit requires a full rotation of the plate over one orbit, while the figure-of-eight does not.

To treat some simple cases where $\boldsymbol{A}$ is not close to the identity, consider the orbits parallel and perpendicular to the direction of current produced. For the parallel orbit (figure 3*c*), let a_+ and a_- be the values taken by $A_{11}(t)$ during motion to the right and left respectively. From the constancy of the rate of dissipation we obtain the exact expression corresponding to the approximation (38),

$$\eta = \left[l\int_0^l A_{ij}\tau_j\,\mathrm{d}s\right]\left[\int_0^l a^{\frac{1}{2}}\,\mathrm{d}s\right]^{-2}, \tag{41}$$

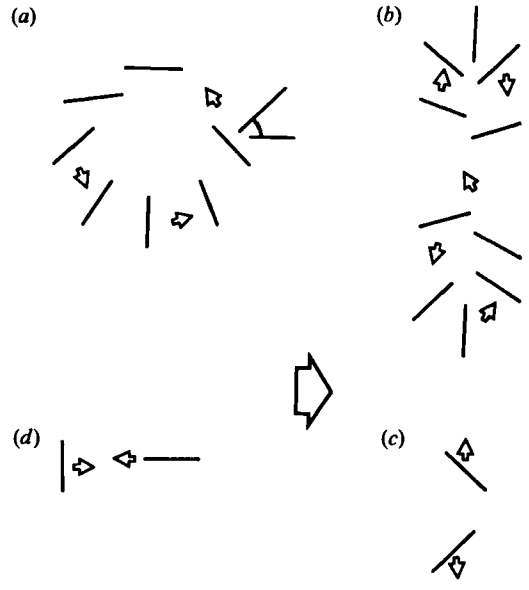

FIGURE 3. Optimal orientations in first-order scanning with $\boldsymbol{A}$ near unity, represented by successive positions of a flat plate. All orbits have approximately the same efficiency. The scanning current, indicated by the large arrow, is to the right. (*a*) Circular orbit, (*b*) figure-of-eight, (*c*) parallel orbit, (*d*) perpendicular orbit.

where $a(t)$ is defined by

$$\boldsymbol{\xi}^s \cdot \boldsymbol{A} \cdot \boldsymbol{\xi}^s = |\xi|^2 a.$$

We must then maximize

$$\eta = \left[l \int_0^{\frac{1}{2}l} (a_+ - a_-)\, \mathrm{d}s \right] \left[\int_0^{\frac{1}{2}l} (a_+)^{\frac{1}{2}} + (a_-)^{\frac{1}{2}}\, \mathrm{d}s \right]^{-2}, \tag{42}$$

and this is accomplished by taking $a_\pm = \lambda_\pm$. For the orbit that is perpendicular to the direction of the current produced (figure 3*d*), we similarly are led to maximize A_{12}/A_{22}, which we do by setting $\cos 2\theta = \beta/\alpha$. We thus obtain the optimal efficiencies

$$\eta = \eta_{\mathrm{H}} = \frac{2(\lambda_+^{\frac{1}{2}} - \lambda_-^{\frac{1}{2}})}{\lambda_+^{\frac{1}{2}} + \lambda_-^{\frac{1}{2}}} \text{ (parallel)}, \tag{43a}$$

$$\eta = \eta_{\mathrm{V}} = \frac{\lambda_+}{2} \frac{-\lambda_-}{(\lambda_+ \lambda_-)^{\frac{1}{2}}} \text{ (perpendicular)}. \tag{43b}$$

If the appendage moved in the same direction as the current (to the right in figure 3*c*) with fixed $\boldsymbol{A}$, we would compute from (36) an efficiency of unity. Because the orbit is closed we conjecture that necessarily η as defined by (36) must be < 1. If this is so then (43*b*) implies $\lambda_+/\lambda_- \leqslant (1+\sqrt{3})^2$. The ratio $\eta_{\mathrm{V}}/\eta_{\mathrm{H}}$ is monotone increasing in λ_+/λ_- and so must be less than 1.27 irrespective of body shape. Since perpendicular and parallel orbits might be thought of as two extremes of the possible motions, it seems likely that there is not an appreciable effect of path on efficiency even though $\boldsymbol{A}$ may differ significantly from the identity.

By a somewhat different sequence of steps, and with one additional assumption on $\boldsymbol{A}(t)$, it is possible to prove that the optimal closed orbit and appendage orientation is achieved by the perpendicular motion just described. This result, which we present

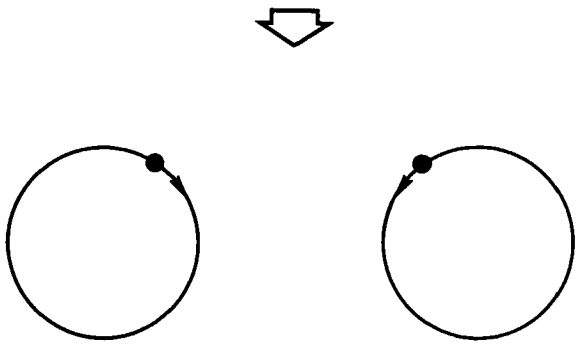

FIGURE 4. Optimal third-order scanning by two spheres. The current is indicated by the large arrow.

in Appendix B, solves a problem of optimal hovering, and is in accord with the usual description of 'normal hovering' at higher Reynolds numbers (Lighthill 1975). However, the bounds on efficiency just noted suggest that a rather large family of orbits of the kind shown in figure 3 have nearly the same efficiency.

We should point out that the definition (25) would not be appropriate for this discussion because it leads to efficiencies that are not homogeneous of degree zero in the $\lambda_{\pm}$, and so would depend upon the meaning of a in (31).

As a last remark concerning first-order scanning, we compare the calculations of this section with a more realistic model of hovering involving several (e.g. two) appendages attached to a body. In the Stokesian realm, the net force on the body is determined by the excess weight and is hence fixed. As the appendages move, the body moves slightly in response to appendage forces not in equilibrium with the gravitational force. Under these conditions we may still ask that the rate of working of the appendages be minimized. While this problem is harder to formulate and solve than the simple one-appendage model which we have considered, similar principles are involved, particularly when the motion is symmetric and allows reduction to a single appendage and the body.

5. Two spheres

We have noted in §2 that the third-order scanning current induced by a sphere moving on a spherical surface will vanish. Recall that third-order scanning is the strongest available mechanism for a simple sphere (specifically, for a body whose resistance is independent of the direction of motion). We show now that two spheres, moving on two non-intersecting spherical surfaces, can efficiently scan at the third-order level. Let the spheres maintain a distance d from the points $(D,0,0)$ and $(-D,0,0)$. We shall assume that the motions are such that the x_1-components of velocity are always of opposite sign and that the x_2- and x_3-components are of the same sign (see figure 4). Adding the effects of both spheres and using this symmetry we have

$$M = 2\int_0^T (D^2 + D\xi_1^{(+)} - D\xi_1^{(-)} + d^2)\,\dot{\xi}_2^{(+)}\,\mathrm{d}t = 4D\int_0^T \xi_1^{(+)}\,\dot{\xi}_2^{(-)}\,\mathrm{d}t, \tag{44}$$

where we set $\boldsymbol{M} = (0, M, 0)$. Minimizing dissipation for fixed M then yields the Euler equations

$$\xi_1^{(+)} + \lambda\dot{\xi}_2^{(+)} = 0, \quad \xi_2^{(+)} - \lambda\dot{\xi}_1^{(+)} = 0. \tag{45}$$

Thus the orbits which close are circular, and lie in the plane determined by the vector $(2D, 0, 0)$ separating the centres of movement, and $\boldsymbol{M}$. We show the optimal motion in figure 4.

To compute the efficiency we use (35), now accounting for both spheres, to obtain

$$\eta = \frac{1}{8\pi^2}\frac{D}{d} = 0.013\frac{D}{d}. \tag{46}$$

For D/d near unity, this is about twice the efficiency of a single sphere moving on the two-circle figure-of-eight path discussed in §2. Note that the unbounded growth of efficiency with D/d is only a result of the irrelevance of path length as an indicator of the radius of the target zone in this configuration, once D/d becomes large. It would perhaps be preferable to take D in place of path length as the target radius, in which case the efficiency is $1/2\pi$.

6. Zero-thrust scanning

A free, neutrally buoyant organism waving appendages at low Reynolds number exerts no net force or moment on the fluid surrounding it. We can then expect the geometry of appendages relative to the body which supports them to affect the scanning strategy and the possible role of swimming. To study some aspects of this problem, consider N Stokeslets carrying forces $\boldsymbol{F}^{(n)}$; if the net Stokeslet strength is zero, the dominant contribution in the far field comes from the Stokes dipoles:

$$u_i \approx -\sum_{n=1}^{N} \frac{\partial S_{ij}}{\partial x_k}(\boldsymbol{x})\,\xi_k^{(n)} F_j^{(n)}, \quad S_{ij} = \frac{1}{8\pi\mu}\left(\frac{x_i x_j}{|\boldsymbol{x}|^3} + \frac{\delta_{ij}}{|\boldsymbol{x}|}\right). \tag{47}$$

We therefore have

$$\frac{1}{T}\int_0^T x_i u_i \,\mathrm{d}t = X_{ik} M_{jk}, \quad X_{jk} = \frac{1}{8\pi\mu|\boldsymbol{x}|}\left(-\delta_{jk} + \frac{3x_j x_k}{|\boldsymbol{x}|^2}\right), \tag{48}$$

$$M_{jk} = \frac{1}{T}\int_0^T \sum_{n=1}^{N} F_j^{(n)}\,\xi_k^{(n)}\,\mathrm{d}t.$$

Since X_{jk} is symmetric, the scanning current is independent of the torque balance, in that contributions come only from the symmetric part of M_{jk}. It is perhaps worth noting that one must impose a torque balance with regard to torque singularities as well as moments of Stokeslets. If a number of appendages are represented as distinct Stokeslets, an instantaneous torque balance of the form

$$\sum_{n=1}^{N} \boldsymbol{\xi}^{(n)} \times \boldsymbol{F}^{(n)} = 0, \tag{49}$$

assumes no torque singularities occur. The latter decay, in the far field of the body represented by a Stokeslet, like $|\boldsymbol{x}|^{-2}$, and have the local form

$$\boldsymbol{T} = \frac{\boldsymbol{\omega}\times\boldsymbol{x}}{|\boldsymbol{x}|^3} \quad (\boldsymbol{\omega} = \text{constant}). \tag{50}$$

(Note that $\boldsymbol{T}$ makes no contribution to the radial drift.) For example, a group of small spinning spheres can be waved about so that (49) is violated at the Stokeslet level, but the resulting contributions of the form (50) can yield a torque balance in the far field of the group. This is because in the latter field the moment of the Stokeslet

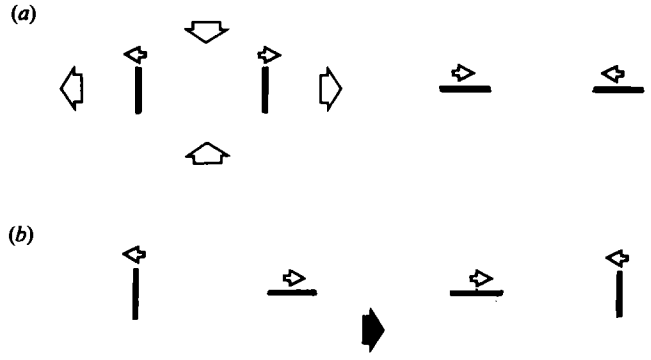

FIGURE 5. Zero-thrust scanning by two Stokeslets, represented by two flat plates moving on a line. (*a*) Scanning mode, with water movement indicated by the large white arrows. (*b*) Swimming mode, with motion to the right, as indicated by the large black arrow.

reduces to a cancelling torque singularity. Therefore, the only new condition to be imposed on the extremal problem is

$$\sum_{n=1}^{N} \boldsymbol{F}^{(n)} = 0. \tag{51}$$

6.1. *Two Stokeslets moving on a line*

Some of the questions which arise in this case can be seen in the motion of two Stokeslets along a line. Let $\xi_A(t), \xi_B(t)$ be the scalar positions of two bodies moving on a line, with friction coefficients (defined analogously to the matrix $\boldsymbol{A}$ in (31)) A and B. The motion will consist of two events (see figure 5): for a time interval T_1, $\dot{\xi}_A$ is positive and $\dot{\xi}_B$ is negative, with coefficients A_1, B_1. During a subsequent time interval of duration T_2, $\dot{\xi}_A$ is negative and $\dot{\xi}_B$ positive, with coefficients A_2, B_2. Except for signs these are all arbitrary functions of time.

From the force balance (51) we have $A\dot{\xi}_A + B\dot{\xi}_B = 0$ or $\dot{\xi}_B = -B^{-1}A\dot{\xi}_A$. The rate of dissipation is given by

$$\frac{W}{T} = 6\pi\mu a(A\dot{\xi}_A^2 + B\dot{\xi}_B^2) \equiv 6\pi\mu a k. \tag{52}$$

Since k is constant on an optimal orbit, we have

$$\dot{\xi}_A = \frac{(a_1 k)^{\frac{1}{2}}}{A_1} \equiv u_1(t) \quad (0 \leqslant t_1 < T_1), \tag{53a}$$

$$\dot{\xi}_B = -\frac{(a_2 k)^{\frac{1}{2}}}{A_2} \equiv -u_2(t), \quad T_1 \leqslant t < T_1 + T_2 = T, \quad \alpha_i = \frac{A_i B_i}{A_i + B_i}. \tag{53b}$$

We next fix the total excursion and assume

$$\int_0^{T_1} (\dot{\xi}_A - \dot{\xi}_B)\,\mathrm{d}t = L = -\int_{T_1}^{T} (\dot{\xi}_A - \dot{\xi}_B)\,\mathrm{d}t. \tag{54}$$

Therefore

$$\int_0^{T_1} u_1(t)\,(1 + B_1^{-1} A_1)\,\mathrm{d}t = L = -\int_{T_1}^{T} u_2(t)\,(1 + B_2^{-1} A_2)\,\mathrm{d}t$$

$$= \int_0^{T_1} \left(\frac{k}{\alpha_1}\right)^{\frac{1}{2}} \mathrm{d}t = \int_{T_1}^{T} \left(\frac{k}{\alpha_2}\right)^{\frac{1}{2}} \mathrm{d}t. \tag{55}$$

From (48) the scanning field has radial component

$$\frac{3\cos^2\theta-1}{|x|^2}\frac{3a}{4T}\int_0^T (A\xi_A\dot{\xi}_A+B\xi_B\dot{\xi}_B)\,dt. \tag{56}$$

Since this is the radial component, the scanning current can be described as having the general character of a Stokes dipole (or a harmonic quadrupole), as determined by the orientation of the flow lines (see figure 5). In the use of 'dipole' below we adhere to the classification by Stokes solutions. We now compute

$$\begin{aligned}\dot{V}_{\text{scan}} &= \frac{2\pi a}{\sqrt{3}}\frac{1}{T}\int_0^T (a\xi_A\dot{\xi}_A+B\xi_B\dot{\xi}_B)\,dt \\ &= \frac{2\pi a}{\sqrt{3}}\frac{1}{T}\left[\int_0^{T_1}(\xi_A-\xi_B)(\alpha_1 k)^{\frac{1}{2}}\,dt-\int_{T_1}^T(\xi_A-\xi_B)(\alpha_2 k)^{\frac{1}{2}}\,dt\right].\end{aligned} \tag{57}$$

Using (55), (57) takes the form

$$\begin{aligned}\dot{V}_{\text{scan}} = \frac{2\pi a}{\sqrt{3}}\Bigg[&\frac{1}{T}\int_0^{T_1}\left(L_0+\int_0^t\left(\frac{k}{\alpha_1}\right)^{\frac{1}{2}}dt'\right)(k\alpha_2)^{\frac{1}{2}}\,dt \\ &-\frac{1}{T}\int_{T_1}^T\left(L_0+L-\int_{T_1}^t\left(\frac{k}{\alpha_2}\right)^{\frac{1}{2}}dt'\right)(k\alpha_2)^{\frac{1}{2}}\Bigg]dt,\end{aligned} \tag{58}$$

where L_0 is the initial separation of the Stokeslets. Physically it is obvious that if the configuration of Stokeslets is not to undergo a net displacement over one period we must have $A_1 = B_1$ and $A_2 = B_2$. In this case the optimal orientations are the extreme ones; that is, if A_i and B_i lie between λ_- and λ_+ then either $A_1 = B_1 = \lambda_+, A_2 = B_2 = \lambda_-$, or the other way around, the only difference being the sign of the scanning field. In the former case we obtain from (58)

$$T_1 = L\left(\frac{\lambda_+}{2k}\right)^{\frac{1}{2}},\quad T_2 = L\left(\frac{\lambda_-}{2k}\right)^{\frac{1}{2}},\quad \dot{V}_{\text{scan}} = \frac{\pi a L^2}{2T\sqrt{3}}(\lambda_+-\lambda_-)\left(1+\frac{2L_0}{L}\right) \tag{59}$$

$$\eta_{\text{scan}} = \frac{4\mu\dot{V}_{\text{scan}}}{W} = \frac{2}{3\sqrt{3}}\left(\frac{(\lambda_+)^{\frac{1}{2}}-(\lambda_-)^{\frac{1}{2}}}{(\lambda_+)^{\frac{1}{2}}+(\lambda_-)^{\frac{1}{2}}}\right)\left(1+2\frac{L_0}{L}\right). \tag{60}$$

To consider the opposite case, where the system swims without generating a scanning dipole field, we set $A_1 = B_2 = \lambda_-, B_1 = A_2 = \lambda_+$. The system will then swim to the right with speed

$$U_{\text{swim}} = \frac{L}{T}\left(\frac{\lambda_+-\lambda_-}{\lambda_++\lambda_-}\right). \tag{61}$$

The resulting flux into a target zone of radius R is

$$\dot{V} = \pi R^2 U_{\text{swim}}, \tag{62}$$

and the efficiency of particle capture by swimming is therefore (with the new values of $T_{1,2}$ computed from (55)),

$$\eta_{\text{swim}} = \frac{R^2}{24aL}\left(\frac{\lambda_+-\lambda_-}{\lambda_++\lambda_-}\right). \tag{63}$$

If, for example, we set $L_0 = \frac{1}{2}L, \lambda_- = \lambda_0 = \frac{1}{2}\lambda_+$, we obtain

$$\frac{\eta_{\text{scan}}}{\eta_{\text{swim}}} = 6.17\frac{a\lambda_0 L}{R^2}. \tag{64}$$

If we assume the excursion L and $a\lambda_0$ are of the order of about half the length of the organism, then (64) suggests that swimming should be the preferred strategy when the target zone is larger than the body. If the organism is able to locate a food particle several body lengths away, and if food is widely dispersed, the preferred strategy would be to swim at random until a particle is sensed, then to home in on it.

This calculation has neglected, however, the likely presence of a large inert body to which the Stokeslet-producing appendages might be attached. One can imagine that the body could act like a sea anchor and render the swimming behaviour inefficient compared to scanning, simply because of the effort then required to displace the entire organism. To verify this we shall assume that interaction between the appendages and the body can be neglected. While this is unreasonable for detailed analysis of the scanning currents produced, it is acceptable for assessing the importance of body drag during swimming. It then follows that η_{scan} is unaffected by the body for the symmetric motion of appendages considered above. For swimming, on the other hand, the body will affect the rate of dissipation. The latter is now given by

$$\frac{W}{6\pi\mu aT} = \left(\frac{L}{T} - U_{\text{swim}}\right)^2 \lambda_+ + \left(\frac{L}{T} + U_{\text{swim}}\right)^2 \lambda_- + U_{\text{swim}}^2 \lambda_{\text{body}},$$

where λ_{body} is the resistance coefficient of the added body. Using (61) and (62) we then see that, with the body included, (63) is changed to

$$\eta_{\text{swim}} = \frac{R^2}{6aL}\left(\frac{\lambda_+ - \lambda_-}{\lambda_+ + \lambda_-}\right) K_{\text{body}}, \tag{63*}$$

$$K_{\text{body}} = \left[\frac{4\lambda_+\lambda_-}{\lambda_+ + \lambda_-} + \left(\frac{\lambda_+ - \lambda_-}{\lambda_+ + \lambda_-}\right)^2 \lambda_{\text{body}}\right]^{-1}.$$

For the parameter values above (64) this results in a new factor $(1+\lambda_{\text{body}}/24\lambda_0)^{-1}$. While admittedly crude, this estimate suggests that body resistance must be quite large compared to appendage resistance before it will be determining on the efficiency of a scanning strategy. It must be noted however, that we have neglected the possible reduction of appendage efficiency because of interaction of the scanning field with the body.

The efficiency (60) would suggest that scanning could be improved without limit by making L small compared to L_0. However the far-field approximation has been used to compute the scanning amplitude. To hold the letter fixed while minimizing dissipation is equivalent to holding $L_0 L$ fixed while minimizing L^2. Ultimately the two appendages act on the target zone as two independent Stokeslets, rather than as a single Stokes dipole, at which point the dissipation increases. For any fixed target zone, there will then be an optimal value of L_0/L.

The above computations of η_{scan}, for linear motion of Stokeslets, is sufficiently simple to allow a test of constant rate of dissipation as a criterion for an optimal behaviour. Let us suppose that the Stokeslets move in the scanning mode as before, except that the outward and inward movements take arbitrary times T_+, T_- where $T_+ + T_- = T$. It is then not difficult to show that the expression for the efficiency (60) is modified by the factor

$$\frac{((\lambda_+)^{\frac{1}{2}} + (\lambda_-)^{\frac{1}{2}})^2}{\lambda_+ T/T_+ + \lambda_- T/T_-}.$$

The maximum value of this factor is 1, occurring when $T_-/T_+ = (\lambda_-/\lambda_+)^{\frac{1}{2}}$. If, for example, we take $\lambda_+/\lambda_- = 1.5$, a not unreasonable value given the relative insensi-

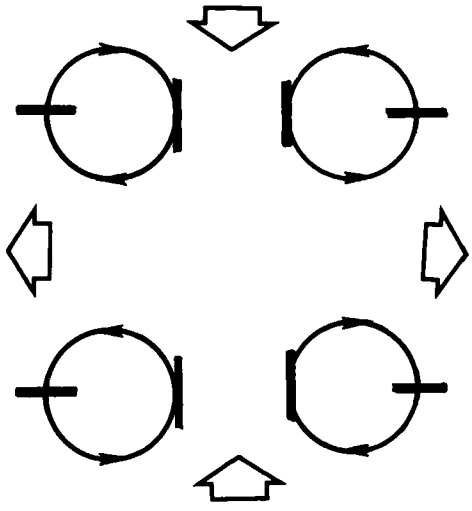

FIGURE 6. An example of a second-order quadrupole field, produced by two pairs of appendages. Phases and resistances are indicated. The water movement is in the direction of the large white arrows.

tivity of Stokes resistances to cross-section, we find that the optimal value of 1 at $T_-/T_+ = 0.82$ reduces to only 0.99 at 1 and 0.96 at 1.25. To lower the figure of 0.99 for constant speed to the relatively costly value of $0.80, \lambda_+/\lambda_-$ must be 9, an unreasonable value in Stokes flow. In spite of the very special system we are considering, the indication is that the optimal speed is not nearly as critical as, say, the issue of paired versus unpaired appendages. The efficiency is about the same over a range of behaviours including movements which are, in a sense, opposite to the optimal one.

When one attempts to find simple examples of second-order scanning which involve realistic configurations of appendages, it is natural to consider immediately at least two appendages, since by symmetric movements there can be cancellation of forces parallel to one axis of the dipole scanning field. If the appendages are attached to a body, the latter will move slightly because of the uncompensated force along an orthogonal axis. A symmetric arrangement of four appendages can be found which balances in two orthogonal directions, if e.g. two-dimensional waving of flat plates is considered. In these hypothetical cases the second-order nature of the scanning will come from a variable resistance of the appendages at different points in the cycle of motion, since waving spheres, for example, whose resistance is the same in all directions, produce third-order scans at best (cf. §2). The manner in which four appendages can generate a second-order quadrupole scanning field is suggested in figure 6.

7. Scanning near a plane boundary

Suppose that we move a sphere on a closed orbit in the vicinity of an infinite plane boundary where the fluid adheres. The scanning field is then altered by the image solution which is needed to satisfy the boundary condition. To first order the sphere may be replaced by a Stokeslet and the analysis of Blake (1972) applies. If x_3 is orthogonal to the plane and $\xi_3(t)$ is the distance of the sphere from the plane, it then

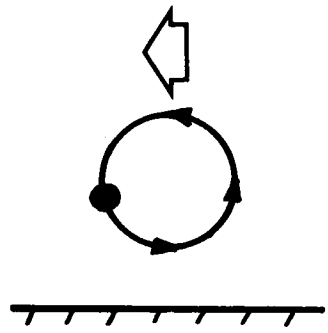

FIGURE 7. Circular motion of an appendage near a rigid plane boundary. The direction of the current is indicated by the large white arrow.

follows that in the far field the dominant flow is proportional to ξ_3 and is due to the components of the motion parallel to the plane. Restricting the orbit to the (x_1, x_3)-plane, the radial flow which results is given by

$$x_i U_i = 9a\xi_3 \dot{\xi}_1 \frac{x_1 x_3}{|\boldsymbol{x}|^3} + O(|\boldsymbol{x}|^{-2}). \tag{65}$$

Thus we have an instance of second-order scanning, with

$$\dot{V} = 9a \frac{1}{T} \int_0^T \xi_3 \dot{\xi}_1 \, \mathrm{d}t. \tag{66}$$

The resulting scanning flow is indicated in figure 7. It is easy to show that the optimal orbit is circular, and, assuming there is no intersection with the boundary, the efficiency defined by (35) is $3/2\pi^2 = 0.15$. We may consider a circular orbit which intersects the boundary provided that we close the orbit by moving the sphere along the plane boundary in a straight line. This closure contributes nothing to the scanning field, but it does contribute to dissipation. Indeed, if the distance to the sphere is of the order of the sphere radius a there will be enhanced dissipation from wall interaction.

If certain appendages of an organism are small in relation to others, or if they operate closer to the body surface than to other appendages, then they may operate almost independently, their main interaction being with the body. In this case we might expect to make use of the simplest wall-interference models to understand the movements.

8. Stalks and flagella

The feeding appendages of many small animals (such as planktonic arthropods) are stalk-like appendages from which emerge long slender filaments, called 'setae'. As a first approximation to this geometry we might take any such appendage to be a single rigid straight stalk with the possibility of some variation in friction coefficient. Of independent interest is the waving of a slender, flexible filament as a model for a flagellum or a cilium. In the present discussion we shall adopt the classical Gray–Hancock theory (Lighthill 1975). This approach, modified to include the interactions between waving appendages, was used by Blake (1972) to study ciliated surfaces. It was also used by Pironneau & Katz (1974) to study optimal movements of a single flagellum.

The hydrodynamics of flagellar motions with application to the feeding of sessile organisms has been discussed by Lunec (1975) and, in a series of papers, by Higdon (1979*a–c*). In the latter work the role of boundary and body is partially accounted for through the Green function for a spherical body above a rigid plane. Using slender-body theory, Higdon considers a flagellum oriented normal to the plane and attached to the outermost point of the sphere, extending outward into a half-space of fluid. The flow set up by waves of a given form is determined numerically, and optimization is done numerically over the geometry of and the parameters of the wave. In the classification of the present paper Higdon thus studies a first-order scanning system, and it can be compared with other systems involving artificially tethered organisms (see §9).

In the present section our object is briefly to describe some results for elongated appendages obtained in simple models of the kind we have used above. We first formulate the problem for an arbitrary continuous linear stalk attached to the origin in an infinite expanse of fluid. We denote the locus of points on the appendage by $\boldsymbol{x}(s,t)$, where $s, 0 \geqslant s \geqslant L$, is the arc length. Assuming that the leg or flagellum is inextensible, s becomes a Lagrangian coordinate for linear position which is a variable independent of t. The condition of inextensibility is then

$$\left|\frac{\partial \boldsymbol{x}}{\partial s}\right|^2 = 1 \quad (t \geqslant 0). \tag{67}$$

According to Gray–Hancock theory, the force per unit length experienced by a waving linear appendage thin in cross-section compared to a typical radius of curvature along its axis, is given by two resistance coefficients $C_{\mathrm{N,T}}$ by

$$\boldsymbol{F} = M^{\cdot}\boldsymbol{x}, \quad M_{ij} = (C_{\mathrm{T}} - C_{\mathrm{N}})\tau_i\tau_j + C_{\mathrm{N}}\delta_{ij}, \quad \boldsymbol{\tau} = \frac{\partial \boldsymbol{x}}{\partial s}. \tag{68}$$

In general the resistance coefficients will be time-dependent since the geometry of filaments, bristles, etc. might be subject to variation over an orbit.

Our problem is then to minimize

$$W = \int_0^T \int_0^L \dot{\boldsymbol{x}}^{\cdot} M^{\cdot} \dot{\boldsymbol{x}}\, \mathrm{d}s\, \mathrm{d}t. \tag{69}$$

In an unbounded fluid the scanning is first-order, and if the Stokeslet field is oriented along the x_1-axis we will fix

$$f = \int_0^T \int_0^L F_1\, \mathrm{d}s\, \mathrm{d}t \quad \text{(Problem 1)}. \tag{70}$$

If the appendage is regarded as situated above the rigid plane $x_3 = 0$, then from §7 we have

$$g = \int_0^T \int_0^L x_3 F_1\, \mathrm{d}s\, \mathrm{d}t \quad \text{(Problem 2)} \tag{71}$$

as our measure of scanning amplitude. Note that for a rigid straight stalk with constant C_{N} problem 1 becomes equivalent to the motion of a sphere on a spherical surface; we know from §2 that there is then no radial scanning current to any order. If C_{N} is allowed to vary, the problem is equivalent to a three-dimensional version of the sphere problem of §4, to which must be added the constraint that the motion be on a spherical surface.

If the stalk is flexible and attached to the plane boundary, our problem is similar to that of fluid transport by cilia (Blake 1972). The observed movement of a cilium involves an almost stalk-like 'effective' stroke, followed by a return stroke nearer

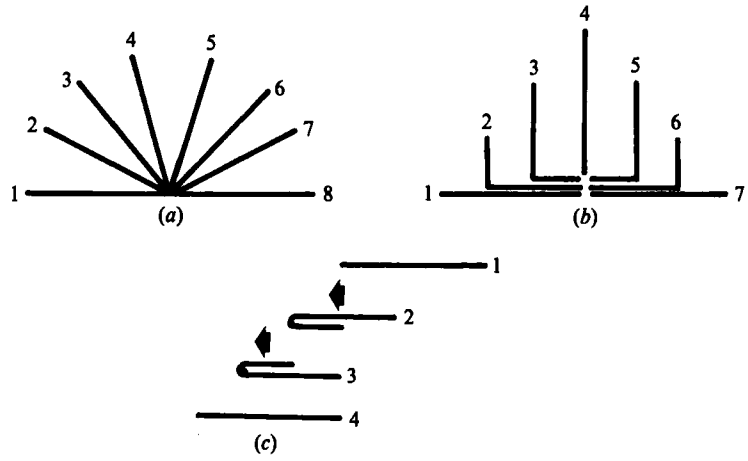

FIGURE 8. Candidates for optimal scanning by a flexible, inextensible filament. (*a*) and (*b*) are effective strokes, and (*c*) is the return stroke. Numbers next to each filament indicate the order in which they assume each position. Arrows indicate the direction of filament motion. The dots indicate the attachment of the filament to the boundary. In (*a*) and (*b*) the images are superimposed, but in (*c*) they are spread out for clarity.

the wall. The effective stroke tends to emphasize C_N, while the return stroke involves, in some instances, largely tangential motion and a force determined by the somewhat smaller coefficient C_T. A beating movement of this kind can cause points along the appendage to move on closed orbits resembling ellipses or circles, so such points might be compared to the sphere moving near a boundary, as discussed in the preceding section. This raises the question of whether boundary interaction of this kind is largely determining on optimal movements, or whether both the boundary effect and distinct friction coefficients are involved.

A good candidate for optimality in either (70) or (71), which is suggested by the form of the observed effective and return strokes noted above, is shown in figure 8(*a*, *c*). In problem 1 with $C_N > C_T > 0$, there is some countercurrent created by the return stroke. In problem 2 the return stroke creates no countercurrent but the value assigned to C_T should include the effect of wall interference. We show in figure 8(*b*) another candidate for an optimal effective stroke, suggested to us by Pironneau, which arises in a related problem of optimal swimming (Pironneau & Katz 1974). In the following we consider the four combinations involving either (70) or (71) and with effective strokes (*a*) or (*b*) in figure 8, which we indicate by appropriate sub and superscripts. As noted by a referee, there are physical restrictions on the bending of actual cilia which would necessarily modify these optima away from the completely flexible movements.

If we define efficiencies

$$(\eta_1, \eta_2) = \frac{(Lf, g)}{TW}, \tag{72}$$

then it is not difficult to calculate $\eta_i^{(a,b)}$ corresponding to the two motions shown in figure 8. We obtain, with $\rho = C_T/C_N$,

$$\eta_1^{(a)} = \frac{3}{\pi^2}\frac{(1-\rho)}{\left(1+\frac{4}{\pi}(\tfrac{1}{3}\rho)^{\frac{1}{2}}\right)^2}, \quad \eta_1^{(b)} = \frac{9}{16}\left(\frac{1-\rho^{\frac{1}{2}}}{1+\rho^{\frac{1}{2}}}\right), \tag{73a}$$

$$\eta_2^{(a)} = \frac{1}{2\pi}\left(1+\frac{4}{\pi}(\tfrac{1}{3}\rho)^{\frac{1}{2}}\right)^{-2}, \quad \eta_2^{(b)} = \tfrac{3}{16}(1+\rho^{\frac{1}{2}})^{-2}. \tag{73b}$$

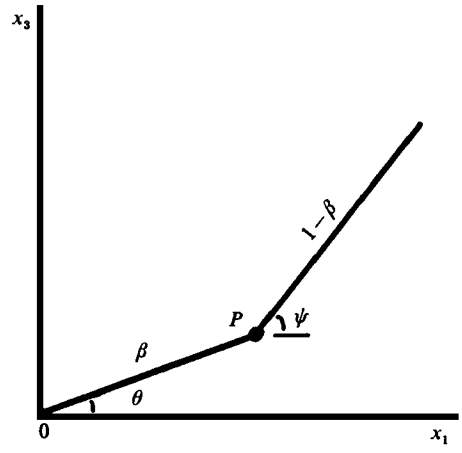

FIGURE 9. A jointed appendage consisting of two straight stalks of lengths $\beta(t)$ and $1-\beta(t)$.

In these computations we have repeatedly used the constancy of the optimal rate of dissipation. We also note that hydrodynamic interactions between different points on the stalk have been neglected, even though in a motion such as the return stroke these would be appreciable.

For the case without boundary, (73a) shows that motion (b) (by which we mean the effective stroke in figure 8b together with the return stroke of figure 8c) is preferred for all ρ, and for the typical value $\rho = 0.7$ we have $\eta_1^{(a)} = 0.035$, $\eta_1^{(b)} = 0.050$. In the case of a plane boundary, motion (a) is preferred provided that $\rho > 0.2$. With $\rho = 0.7$ we have $\eta_2^{(a)} = 0.061, \eta_2^{(b)} = 0.056$. For $\rho = 1$, $\eta_2^{(a)} = 0.053, \eta_2^{(b)} = 0.047$. Thus there is a very weak effect of ρ, which suggests that boundary effects are more important to the scanning strategy than the intrinsic hydrodynamics of a stalk. If we take $\rho = 1$, the points on the stalk behave essentially like spherical bodies and so the theory is a continuous version of the scanning problem considered in §7. The fact that biological appendages are attached to boundaries and sometimes have motions resembling (a) could imply that the comparably modest improvement in efficiency over motion (b) may be of consequence to the organism. However any hinged appendage swung from the base by muscles would more readily do (a) than (b), and so be a consequence of morphology rather than hydrodynamic performance.

The solution of the constrained minimization problem (67)–(69) with (70) or (71) is not an easy matter for general flexible filaments. Perhaps the simplest geometry which is capable of describing a family of realistic movements is that shown in figure 9. The appendage consists of two straight stalks joined at the point P. By allowing the point P to move as a function of time, the two motions of figure 8 can be realized, along with a large family of intermediate cases.

We shall not pursue this line of investigation here, but will summarize some results for small perturbations of a uniformly rotating stalk when the point P is not allowed to move, as would be the case for an anthropod appendage with one joint. Let the two segments of the stalk have, in suitable units, lengths β and $(1-\beta)$. The system is hinged at 0 and P and we assume the appendage remains in the (x_1, x_3)-plane. The angles θ and ψ are defined in figure 9. If, using (69) and (70) we seek extrema of $W+\lambda f$ in this problem, we observe that

$$\theta_0 = \psi_0 = -\pi + 2\pi t \tag{74}$$

are solutions of the Euler equations, with $f = 0$. If we seek nearby extremals by perturbing in an amplitude parameter ϵ, there results

$$\theta = \theta_0 + \epsilon A \cos 2\pi t, \tag{75a}$$

$$\psi = \psi_0 + \epsilon B \cos 2\pi t, \tag{75b}$$

where A and B are functions of $\rho = C_T/C_N$ and β. We can then calculate an efficiency using (72), and then an optimal β for given ρ ($\beta = 0.48$ for $\rho = 0.5$). A similar analysis is possible for a filament rotating above a plane wall ($\beta = 0.75$ for $\rho = 0.5$).

These solutions are, however, far from the motions shown in figure 8, which depend very much upon the motion of the point P. Ideally, the two-stalk system with variable P might provide an effective cilium model provided that wall-dependent C_T and C_N were used, but this leads to a difficult minimization problem, about which little is known. For $0 < \rho < 1$ in the absence of a wall, we conjecture that (*b*), (*c*) of figure 8 is the optimal scanning movement in the two-stalk model, as determined from the efficiency (72).

9. Discussion

The various scanning mechanisms described above provide the beginnings of a framework within which the appendage movements of small aquatic organisms can be analysed. The models predict some interesting biological consequences of the physical properties of these scanning systems.

9.1. *Organisms to which our models apply*

Since Stokes equations have been used throughout, our models are formally restricted to scanning appendages for which inertial effects can be ignored. Stokesian mechanics should however be applicable to the flagella and cilia of protozoans and to many invertebrate larvae (see e.g. the reviews by Chia *et al.* 1981; Fenchel 1986). On the other hand, the scanning appendages of many other abundant small aquatic animals (such as copepods and cladocerans, which are important in marine and freshwater food webs) operate at Reynolds numbers approaching unity (e.g. Lochead 1977; Koehl 1984). In this range, we do not expect the inertial corrections to the present results to be large, for the reasons mentioned in §3 as well as by comparison of the problems considered here with certain classical results, such as the inertial correction to the Reynolds number dependence of the drag of a sphere in uniform motion (see e.g. Batchelor 1967 p. 234). Since viscous stresses are surely significant, it seems to us reasonable to deal with the awkward *Re* range from the low rather than from the high side, at least in these preliminary models.

The scanning behaviours of many small organisms involve complex motions of a number of appendages, often working in concert and close to the body. The combined flow field is not easily modelled by any one of our examples, but the simple geometries we have considered suggest a list of elementary scanning movements involving spheres and stalks. Even a relatively simple subsystem of an organism's scanning, such as the symmetric flapping of two appendages, can combine two or more of the elementary models. For example, all appendages could produce a first-order component in the case of a negatively-buoyant organism. Simultaneously, phases and motions can be coordinated to produce second- or third-order components in the far field, which can create currents as large as the first-order one in the region of the animal.

Although the motivation of the present paper was in scanning as a feeding behaviour, dissolved oxygen and other substances which could also be of importance to the animal are carried by the same current. Hence our models could apply as well to the efficiency of refreshing the water supply of a suitable target zone near the organism. (Gavis 1976 has discussed the diffusion of dissolved substances to the surfaces of small planktonic organisms.)

9.2. *Efficiency*

Our models address the energy efficiency of scanning (volume of water processed per unit of energy expended) for each of a number of mechanisms by which flapping appendages can move fluid. One general result is the constancy of the rate of viscous dissipation at the optimum, throughout the cycle of motion. We have seen, however (§6) that the energy penalty for departures from the optimum may be extremely small. Therefore, we suggest that the 'fine tuning' of rate of dissipation for a fixed cycle of movement may be unimportant through evolutionary time.

In contrast, our models point out certain changes in scanning systems that do produce significant changes in the estimated efficiency (such as the addition of a second appendage, roughly doubling the efficiency in the example of third-order scanning given in §5). Nonetheless, we need to keep in mind that certain aspects of scanning systems may not represent optimization over evolutionary time. For example, although our study suggests that paired appendages can operate more efficiently for scanning than isolated ones, their common occurrence on scanning organisms may simply be the result of bilateral symmetry of non-scanning ancestors of these creatures.

Which scanning mechanisms are most efficient? Although we reiterate that specific instances of scanning must be examined in more detail before any firm conclusions can be drawn concerning the relative benefits of the mechanisms of various orders, the crude estimates suggest a range of possibilities. If a is the appendage's size and L is the size of the orbit, and if we make the extreme assumption that the scanning current into a target volume of roughly R^3 can be evaluated using the far-field scanning velocity, then the volume of water processed per unit time by an nth-order scanner is $V \approx L^n aR^2/TR^n$. The rate of working is $W/t \approx \mu aL^2/T^2$. The efficiency $\eta = \mu \dot{V}/W$ is then approximately $(L/R)^{n-2}$. Roughly, therefore, first-order scanning is preferred for large R/L, third- and higher-order for small R/L, with second-order scanning indifferent to this ratio.

If the energetic cost per unit time to produce a feeding current is small relative to the total metabolic rate of an organism (e.g. Vidal 1980; Fenchel 1986), factors other than energy efficiency may have been more important in the evolution of scanning motions. Perhaps for organisms living in water where food concentrations are low (such as the open ocean, e.g. Conover 1981) and where they must compete for these limited resources with other suspension-feeders, the important optimization problem to consider is maximization of feeding rate, presumably with any number of side conditions. We have considered here only maximization of feeding rate as measured by volume of water processed per unit time relative to scanning work. Another factor that might affect the relative success of a scanning behaviour is the organism's susceptibility to predation during scanning. We have not addressed these issues in this paper, but we can use our models to treat some aspects of predator avoidance.

9.3. *Predator avoidance*

Many invertebrate predators on planktonic organisms sense the presence of their prey by mechanoreception (e.g. Gerritsen & Strickler 1977; Gill & Crisp 1977). Therefore, prey can be cryptic to those predators by disturbing the fluid around themselves as little as possible (e.g. Zaret 1980). Hence, a trade-off may exist between maximizing food captured and minimizing the chances of being captured by a predator. Moreover, as a referee points out, a small-disturbance strategy could also be useful to a predator! This situation has some interesting fluid-mechanical consequences.

In general terms we may conclude that the more rapidly the fluid disturbance decays with distance from a suspension-feeding organism, the more cryptic it is likely to be to predators using mechanoreception. In our analysis we have focused on the radial component of the flow fields produced by various appendage motions since these are the components bringing food into the target zone. We have classified these scanning mechanisms as first-, second-, and third- or higher-order to indicate how this radial component decreases with distance from the animal. However, in analysing cryptic behaviour, non-radial components of the scanning current must be considered as well. One result of this is that third-order scanning behaviours produce a current which decays at the same rate as for general second-order mechanisms (but the slowly-decaying component of this current will move particles on a fixed spherical surface without bringing them closer to the target zone). Therefore, we can predict that first-order scanners will be more noticeable to predators than second-, third-, or indeed higher-order scanners, and that all orders greater than one are similar in this regard.

9.4. *Feeding strategies*

The paths along which planktonic organisms should swim in order to maximize encounter probabilities with food while minimizing encounters with predators have been modelled (e.g. Gerritsen & Strickler 1977), while other studies (e.g. Cowles & Strickler 1983) have focused on how these creatures apportion their time between various behaviours to maximize net energy gain under different conditions of food-particle availability. Hydrodynamic models such as those considered in this paper may help in this analysis of feeding behaviour. For example, we have noted in §6 that scanning and swimming can each be preferred feeding strategies depending upon the relative sizes of target zone and animal. Predictions of this kind may be quite robust within the models considered here.

Another point of interest concerns the combining of models of first-order scanning and hovering into a single theory of optimal feeding behaviour. Haury & Weihs (1976) have argued on the basis of a fluid-dynamical model that the optimum strategy for maintaining vertical position is not steady hovering, but is rather a combination of active upward swimming and passive sinking. Whether this strategy has other significance in terms of scanning or predator avoidance is unclear, but an analysis would seem feasible along the general lines developed here.

9.5. *Effects of gravity, tethering, and sea anchors on scanning*

Biologists have suggested that flow past a scanning organism can be increased by: (i) increasing the negative buoyancy of the organism (Strickler 1982), (ii) tethering the organism (Fenchel 1986), or (iii) increasing the drag on the main body of the organism, so that it acts like a sea anchor to which the scanning appendages are in effect tethered (Emlet & Strathmann 1985). We can consider these suggestions on the basis of the picture we have developed of first-order scanning.

Strictly, only cases (i) and (ii) involve first-order scanning. Mechanism (ii) is of interest because many protozoan feeders actually tether themselves while feeding (Fenchel 1986), and also because tethering is a convenient laboratory procedure for observing an organism during its feeding. How is the flow field altered by this procedure?

When a neutrally buoyant organism swims, the Stokeslet associated with thrust is cancelled by an opposing Stokeslet associated with mean body resistance. These two contributions can be separated mathematically only through a decomposition of the boundary conditions on the moving surfaces. On the other hand, if the organism is held in place by a tether and does not change its flapping behaviour, it will develop a thrust and pull on the tether. The tether force restraining the animal is balanced by a net Stokeslet (i.e. a first-order scanning component) generated by the flapping. We can thus distinguish two cases of tethering, assuming that the leash is invisible to the flow and that the flapping is unaltered by the process: (*a*) if the untethered animal hovers in one spot, the flow field is unaffected by tethering and no force is measured in the leash; (*b*) if the untethered animal swims with speed U, then a force will be measured in the leash and a Stokeslet component is thus added to the flow field produced by the organism. The flow field relative to the animal when tethered would appear as the disturbance field seen around an untethered animal plus that due to a mean drift at speed U in a direction opposite to the force at the tether point. Therefore, the use of a tether can cause a neutrally buoyant swimmer to simulate a relatively heavy first-order scanner, with tether force replacing weight. If a negatively-buoyant organism is tethered, the first-order scanning component can be determined by summing the relative weight and the tether force.

To consider mechanism (iii) above, interpreted as a sea anchor, we must regard the organism as composed of a scanning machine (the flapping appendages) tethered to a high-resistance body (the anchor). In this case there is a distribution of Stokeslets associated with the scanning machine, but it is balanced by another distribution over the body, to make the net Stokeslet strength zero (assuming neutral buoyancy). Only in the immediate vicinity of the scanning machine (where the target zone might be located) will the intense currents associated with local Stokeslets be found, and the existence of an effective sea anchor be confirmed.

In this paper we have outlined a number of basic mechanisms by which waving appendages can produce scanning currents in Stokes flow, and have examined their relative efficiency based upon energy expended to scan a given volume of fluid. The models are very simple and do not account for the complex geometry of feeding organisms. Nevertheless, our analysis clearly indicates the importance of classifying scanning behaviour according to the far-field representation of the current produced. We have also found that optimal scanning movements may fall within a rather broad band of behaviours of essentially equal efficiency. Finally, a number of questions regarding animal behaviour can be studied, including the issue of swimming versus scanning as the most efficient means of feeding.

This research was supported by the National Science Foundation under contracts DMS-831 2229 at New York University (S.C.), OCE-820 1395 and OCE-851 0834 at the University of California, Berkeley (M.K.), and DMS-840 3186 at Duke University (M.M.). M.K. is grateful to J. D. Murray for the use of the facilities of the Centre for Mathematical Biology, University of Oxford (S.E.R.C. of Great Britain, Grant No. GR/DS/13573).

We thank the referees for their comprehensive and constructive criticism.

Appendix A

We shall consider Eulerian and Lagrangian definitions of mean scanning current, at a point $\boldsymbol{x}$ in the far field of a scanning system located near the origin. Let $\boldsymbol{x}_{\mathrm{p}}(t)$ denote the position of a Lagrangian particle initially at $\boldsymbol{x}$. We shall consider the flow over one period T of the scanning system. If $\boldsymbol{u}(\boldsymbol{x}, t)$ is the velocity field created by the system, the Eulerian mean velocity at $\boldsymbol{x}$ is defined by

$$\boldsymbol{U}_{\mathrm{E}} \equiv \frac{1}{T}\int_0^T \boldsymbol{u}(\boldsymbol{x}, t)\,\mathrm{d}t. \tag{A 1}$$

Now the Lagrangian point satisfies

$$\frac{\mathrm{d}\boldsymbol{x}_{\mathrm{p}}(t)}{\mathrm{d}t} = \boldsymbol{u}(\boldsymbol{x}_{\mathrm{p}}(t), t), \quad \boldsymbol{x}_{\mathrm{p}}(0) = \boldsymbol{x}. \tag{A 2}$$

The Lagrangian mean of the particle velocity near the point $\boldsymbol{x}$ is then

$$\boldsymbol{U}_{\mathrm{L}} \equiv \frac{1}{T}\int_0^T \boldsymbol{u}(\boldsymbol{x}_{\mathrm{p}}(t), t)\,\mathrm{d}t. \tag{A 3}$$

This definition is reasonable in the far field since $|\boldsymbol{u}|T \ll |\boldsymbol{x}|$ there.

Comparing the two mean velocities we have

$$\begin{aligned}\boldsymbol{U}_{\mathrm{E}} - \boldsymbol{U}_{\mathrm{L}} &= \frac{1}{T}\int_0^T [\boldsymbol{u}(\boldsymbol{x}_{\mathrm{p}}, t) - \boldsymbol{u}(\boldsymbol{x}, t)]\,\mathrm{d}t,\\ &\approx \frac{1}{T}\int_0^T (\boldsymbol{x}_{\mathrm{p}} - \boldsymbol{x})\cdot\nabla\boldsymbol{u}(\boldsymbol{x}, t)\,\mathrm{d}t,\\ &\approx \frac{1}{T}\int_0^T \int_0^t \boldsymbol{u}(\boldsymbol{x}, t')\,\mathrm{d}t'\cdot\nabla\boldsymbol{u}(\boldsymbol{x}, t)\,\mathrm{d}t.\end{aligned} \tag{A 4}$$

Suppose now that the scanning system involves a single characteristic length L. Then in the far field

$$\boldsymbol{u}(\boldsymbol{x}, t) = U_0 \sum_1^\infty \boldsymbol{T}_n(L^{-1}\boldsymbol{x}, T^{-1}t), \tag{A 5}$$

where $|\boldsymbol{T}_n|$ is homogeneous of degree n in $L^{-1}\boldsymbol{x}$. Thus, from (A 4) we have

$$\boldsymbol{U}_{\mathrm{E}} - \boldsymbol{U}_{\mathrm{L}} = O(U_0^2 T L^2 |\boldsymbol{x}|^{-3}). \tag{A 6}$$

so that, in general, the difference between the Lagrangian and Eulerian definition of mean scanning velocity will appear at the third-order level.

However, scanning systems may involve more than one scale of length. In our example of third-order scanning (§2), a sphere of radius a moves on an orbit of size $L \gg a$. This produces an instantaneous Stokeslet component in $\boldsymbol{u}$ of order $(aL/T|\boldsymbol{x}|)$. Using this in (A 4) we then have

$$\boldsymbol{U}_{\mathrm{E}} - \boldsymbol{U}_{\mathrm{L}} = O(a^2 L^2 T^{-1} |\boldsymbol{x}|^{-3}), \tag{A 7}$$

whereas the radial component of the Eulerian scanning current is of order $aL^3T^{-1}|\boldsymbol{x}|^{-3}$ and so is larger by a factor L/a. More generally, if the scanning is nth-order according to the Eulerian definition (A 1), Eulerian and Lagrangian velocities coincide provided that $aL^n|\boldsymbol{x}|^{-n} \gg a^2L^2|\boldsymbol{x}|^{-3}$, implying the scales must be ordered so that $a \ll L^{n-2}|\boldsymbol{x}|^{3-n}$. In effect the second length allows the particle velocity to be made very small without adjusting the geometry of the scanning orbit.

The above arguments depend only upon orders and so are general. The actual value of $\boldsymbol{U}_{\mathrm{E}}-\boldsymbol{U}_{\mathrm{L}}$ may be smaller in specific instances. For example, for the sphere of constant radius (§2) we find that

$$\boldsymbol{x}\cdot(\boldsymbol{U}_{\mathrm{E}}-\boldsymbol{U}_{\mathrm{L}}) \approx \frac{1}{2T}\int_0^T \frac{\mathrm{d}}{\mathrm{d}t}\left[|\boldsymbol{x}|^{-2}|\delta\boldsymbol{\xi}|^2-5|\boldsymbol{x}|^{-4}(\delta\boldsymbol{\xi}\cdot\boldsymbol{x})^2\right]\mathrm{d}t = 0, \tag{A 8}$$

where $\delta\boldsymbol{\xi} = \boldsymbol{\xi}(t)-\boldsymbol{\xi}(0)$. Thus radial drifts of particles agree to the order of scanning, even though the latter is three.

Appendix B

We shall determine the optimal orbit for the problem of §4. We first suppose that $\boldsymbol{A}(t)$ is given, along with the period T, and seek to find a function $\boldsymbol{q}(t)$ which minimizes dissipations for fixed M on a closed orbit. We thus have the two side conditions

$$\frac{1}{T}\int_0^T \boldsymbol{e}\cdot\boldsymbol{A}\cdot\boldsymbol{q}\,\mathrm{d}t = \frac{M}{T}, \quad \frac{1}{T}\int_0^T q\,\mathrm{d}t = 0, \quad \boldsymbol{e} = (1,0,0). \tag{B 1}$$

Since $\boldsymbol{A}$ is symmetric, the extremal satisfies

$$\boldsymbol{A}\cdot\boldsymbol{q} = \lambda\boldsymbol{A}\cdot\boldsymbol{e}+\boldsymbol{\nu}, \tag{B 2}$$

where λ and $\boldsymbol{\nu}$ are constant multipliers. We may solve for these using (B 1). If $\langle\cdot\rangle$ denotes the time average over one period and $\boldsymbol{S} = \langle\boldsymbol{A}^{-1}\rangle^{-1}$, $\boldsymbol{I}$ = identity, then

$$\begin{aligned}\boldsymbol{q} &= \lambda[\boldsymbol{I}-\boldsymbol{A}^{-1}\boldsymbol{B}]\cdot\boldsymbol{e}, \quad \lambda = \frac{M}{T}[\boldsymbol{e}\cdot(\langle\boldsymbol{A}\rangle-\boldsymbol{B})\cdot\boldsymbol{e}]^{-1}\\ &\equiv \frac{M}{\gamma T}.\end{aligned} \tag{B 3}$$

From (B 3) and (41) we obtain an efficiency

$$\eta = \frac{l\gamma}{M} = \frac{1}{T}\int_0^T |\boldsymbol{e}-\boldsymbol{A}^{-1}\boldsymbol{B}\cdot\boldsymbol{e}|\,\mathrm{d}t. \tag{B 4}$$

We can now optimize over the orbit provided that we restrict attention to functions $\boldsymbol{A}(t)$ satisfying $\langle A_{12}\rangle = 0$. (Equivalent to $\langle\sin 2\theta\rangle = 0$, cf. figure 3). This is the added condition which we referred to at the end of §4. In this case (B 3) takes the form

$$\boldsymbol{q} = \lambda\left[1-\frac{A_{22}}{\langle A_{22}\rangle}, \quad -\frac{A_{12}}{\langle A_{22}\rangle}\right]. \tag{B 5}$$

We now show that A_{22} must be constant on the optimal orbit, given that the invariants of $\boldsymbol{A}$ are independent of time. By the constancy of the rate of dissipation for optimal scanning (§3), we have, using (B 5)

$$A_{11}+(\boldsymbol{B}\boldsymbol{A}^{-1}\boldsymbol{B})_{11} = \text{constant},$$

so either

$$A_{11}+\frac{\mathrm{Det}\,(\boldsymbol{A})\,A_{22}}{\langle A_{22}\rangle^2} = \text{constant},$$

or else

$$\left(1-\frac{\mathrm{Det}\,(\boldsymbol{A})}{\langle A_{22}\rangle^2}\right)A_{11} = \text{constant}.$$

Thus either A_{11} (and therefore A_{22}) is constant, or else $\mathrm{Det}\,(\boldsymbol{A}) = \langle A_{22}\rangle^2$. In the latter case (B 4) and (B 5) give

$$\eta = \left(\frac{\mathrm{trace}\,(\boldsymbol{A})-2(\mathrm{Det}\,(\boldsymbol{A}))^{\frac{1}{2}}}{\mathrm{Det}\,(\boldsymbol{A})}\right)^{\frac{1}{2}}\langle A_{22}^{\frac{1}{2}}\rangle. \tag{B 6}$$

Thus to maximize η in (B 6) we must set A_{22} equal to $(\mathrm{Det}(A))^{\frac{1}{2}}$. This again gives constant A_{22} but with efficiency

$$\eta = \frac{(\lambda_+)^{\frac{1}{2}} - (\lambda_-)^{\frac{1}{2}}}{(\lambda_+ \lambda_-)^{\frac{1}{4}}} \tag{B 7}$$

which is smaller than (43*b*).

We thus find that the optimal orbit is, by (B 5) with A_{22} constant, a vertical one, and the discussion reverts to that given in §4, leading to (43*b*).

REFERENCES

BATCHELOR, G. K. 1967 *An Introduction to Fluid Dynamics*. Cambridge University Press.

BLAKE, J. R. 1971 A note on the image system for a Stokeslet in a no-slip boundary. *Proc. Camb. Phil. Soc.* **70**, 303–310.

BLAKE, J. R. 1972 A model for the micro-structure of ciliated organisms. *J. Fluid Mech.* **55**, 1–23.

BLAKE, J. R., LIRON, N. & ALDIS, G. K. 1982 Flow patterns around ciliated microorganisms and in ciliated ducts. *J. Theoret. Biol.* **98**, 127–41.

CHIA, F. S., BUCKLAND-NICKS, J. & YOUNG, C. M. 1981 Locomotion of marine invertebrate: A review. *Can. J. Zool.* **62**, 1025–1222.

CHWANG, ALLEN T. & YAO-TSU WU, T. 1975 Hydromechanics of low-Reynolds-number flow. Part 2. Singularity method for Stokes flows. *J. Fluid Mech.* **67**, 787–815.

CONOVER, R. J. 1981 Nutritional strategies for feeding on small suspended particles. In *Analysis of Marine Ecosystems* (ed. J. R. Longhurst), pp. 363–395. Academic Press.

COWLES, T. J. & STRICKLER, J. R. 1983 Characterization of feeding activity patterns in the planktonic copepod *Centropages typicus* Kroyer under various food conditions. *Limnol. Oceanogr.* **28**, 106–115.

EMLET, R. B. & STRATHMAN, R. R. 1985 Gravity, drag, and feeding currents of small zooplankton. *Science* **228**, 1016–1017.

FENCHEL, T. 1986 Protozoan filter feeding. In *Progress in Protistology* (in press).

GAVIS, J. 1976 Munk and Riley revisited: Nutrient diffusion transport and rates of phytoplankton growth. *J. Mar. Res.* **34**, 161–179.

GERRITSEN, J. & STRICKLER, J. R. 1977 Encounter probabilities and community structure in zooplankton: a mathematical model. *J. Fish. Res. Board Can.* **34**, 73–82.

GILL, C. W. & CRISP, D. J. 1985 Sensitivity of intact and antennule amputated copepods to water disturbance. *Mar. Ecol. Prog. Ser.* **21**, 221–227.

HAPPEL, J. & BRENNER, H. 1965 *Low Reynolds Number Hydrodynamics*. Prentice-Hall.

HAURY, L. & WEIHS, D. 1976 Energetically efficient swimming behavior of negatively buoyant zooplankton. *Limnol. Oceanogr.* **21**, 797–803.

HIGDON, J. J. L. 1979*a* A hydrodynamic analysis of flagellar propulsion. *J. Fluid Mech.* **90**, 685–711.

HIGDON, J. J. L. 1979*b* The generation of feeding currents by flagellar motions. *J. Fluid Mech.* **94**, 305–330.

HIGDON, J. J. L. 1979*c* The hydrodynamics of flagellar propulsion: helical waves. *J. Fluid Mech.* **94**, 331–351.

JAHNKE, E. & EMDE, F. 1945 *Tables of Functions*. Dover.

KOEHL, M. A. R. 1984 Mechanisms of particle capture by copepods at low Reynolds numbers: possible modes of selective feeding. In *Trophic Dynamics within Aquatic Ecosystems* (eds D. G. Meyers & J. R. Strickler), pp. 135–166. Westview Press.

LIGHTHILL, M. J. 1975 *Mathematical Biofluiddynamics*. SIAM vol. 17, Regional Conference Series in Applied Mathematics, Society for Industrial and Applied Mathematics, Philadelphia.

LOCHEAD, J. H. 1977 Unsolved problems of interest in the locomotion of crustacea. In *Scale Effects in Animal Locomotion* (ed. T. J. Pedley), pp. 257–268. Academic.

LUNEC, J. 1975 Fluid flow induced by smooth flagella. In *Swimming and Flying in Nature* (ed. T. Y.-T. Wu, C. J. Brokaw & C. Brennen), vol. 1, pp. 143–159. Plenum.

PIRONNEAU, O. & KATZ, D. F. 1974 Optimal swimming of flagellated microorganisms. *J. Fluid Mech.* **66**, 391–415.

STRICKLER, J. R. 1982 Calanoid copepod feeding currents, and the role of gravity. *Science* **218**, 158–160.

VIDAL, J. 1980 Physioecology of zooplankton. III. Effects of phytoplankton concentration, temperature, and body size on the metabolic rate of *Calanus pacificus*. *Mar. Biol.* **56**, 195–202.

ZARET, R. E. 1980 The animal and its viscous environment. In *Evolution and Ecology of Zooplankton Communities* (ed. W. C. Kerfoot), pp. 3–9. University Press of New England.